Experimental Performance Analysis (c* & c* efficiency) of a Premixed Green Propellant consisting of N2O and C2H4

Conference Paper · July 2017

CITATIONS
8

READS
961

4 authors, including:

Lukas Werling
German Aerospace Center (DLR)
51 PUBLICATIONS **296** CITATIONS

SEE PROFILE

Experimental Performance Analysis (c^* & c^* efficiency) of a Premixed Green Propellant consisting of N_2O and C_2H_4

Lukas Werling*, Matthias Haßler†, Patrick Bätz‡, Helmut Ciezki§ and Stefan Schlechtriem ¶

German Aerospace Center (DLR), Institute of Space Propulsion, Hardthausen, 74239, Germany

Today hydrazine is the commonly used monopropellant for attitude- and orbit control of satellites and the propellant of choice to power probes or landers. Due to changing political and economic framework, (e.g. the REACH regulation in Europe) different propellants for replacing hydrazine are currently under development or qualification. Aside ADN based propellants, the German Aerospace Center's Institute of Space Propulsion is focusing on mixtures of nitrous oxide and hydrocarbons. The idea is to premix nitrous oxide and a fuel and to store both substances together in a single tank. Those mixtures - so called premixed monopropellants - are non-toxic, provide a significant higher I_{sp} than hydrazine ($\geq$ 300 s) and offer low propellant costs. The biggest challenges concerning those propellants are the immanent danger of flashback across the injection system and the high combustion temperatures (>3000 K). The most known nitrous oxide/fuel mixture is NOFBX ^{TM} by Firestar. DLR calls its mixture HyNOx (Hydrocarbons mixed with nitrous oxide). To gain experience with a propellant mixture consisting of nitrous oxide (N_2O) and ethylene (C_2H_4) and solve the mentioned challenges, DLR is conducting hot gas combustion tests with an experimental combustor. The paper summarizes the results of combustion tests conducted with the premixed propellant injected in gaseous state. The measured performance parameters (c^* and η_{c^*}), depending on mixture ratio and chamber pressure are shown and discussed. Furthermore a test campaign to derive the characteristic combustion chamber length L* is presented. The maximum c^* of about 1550 m/s is obtained with an characteristic chamber length of 0.56m.

Nomenclature

$\dot{m}$	=	Mass flow rate [kg/s]
$\dot{n}_{N2O}$	=	flow of N_2O moles per second [mol/s]
$\dot{Q}_{loss}$	=	Heat loss at chamber walls [MW]
$\dot{q}_{loss}$	=	Heat flux density in combustion chamber [MW/m^2]
A_t	=	Nozzle throat area [m^2]
c^*	=	Charateristic exhaust velocity [m/s]
L^*	=	Characteristic combustion chamber length [m]
L_{seg}	=	Length of combustion chamber segments [m]
p_{cc}	=	Combustion chamber stagnation pressure [bar]
S_{cc}	=	Surface area of the inner combustion chamber walls [m^2]
T_{cc}	=	Combustion temperature [K]

*Head Facilities Group, Institute of Space Propulsion, D-74239 Hardthausen, AIAA Member.

†Master Thesis Student at Institute of Space Propulsion, Technical University of Munich, D-85748 Mnchen.

‡Master Thesis Student at Institute of Space Propulsion, University of Stuttgart, D-70174 Stuttgart.

§Head of Propellants Department, Institute of Space Propulsion, Im Langen Grund D-74239 Hardthausen, AIAA Member

¶Director of the Institute of Space Propulsion, Institute of Space Propulsion, Im Langen Grund, D-74239 Hardthausen, AIAA Senior Member.

V_{cc} = Combustion chamber volume (from injector to nozzle throat) [m^3]
DLR = German Aerospace Center
HPS = Hydrazine propulsion system
I_{sp} = Specific impulse (by weight) [s]
M = Molar mass [kg/mol]
M_{N_2O} = Molar mass of nitrous oxide [kg/mol]
R = Gas constant [J/(K mol)]
ROF = Ratio of the mass flows: oxidizer/fuel
TRL = Technology-Readiness-Level

Symbols

ΔH_l = Enthalpy losses caused by heat flux to the chamber wall [kJ/mol]
$\Delta H^0_{r,l}$ = Reaction enthalpy with losses caused by heat flux to the chamber wall [kJ/mol]
ΔH^0_r = Reaction enthalpy at standard conditions [kJ/mol]
ϵ = Nozzle expansion ratio
η_{c^*} = c^* or combustion efficiency
κ = Ratio of the specific heats c_p/c_v
ρ = Density [kg/m^3]

I. Introduction

For decades hydrazine (N_2H_4) and its derivatives are used to propel satellites, planetary probes or in combination with dinitrogentetroxide (N_2O_4) upper stages. Hydrazine offers sufficient I_{sp} (up to 240 s), is long term storable, can easily be decomposed via catalyst and an explosion of the propellant is very unlikely.[1] Additionally it reacts hypergolic with N_2O_4, which makes an ignition system for upper stages redundant. One the opposite, hydrazine is highly toxic and carcinogenic. Thus the fueling process of a spacecraft is a tedious process with high safety measures. Along with the high precautions, high costs for the overall fueling and transportation process occur. As a consequence of hydrazine's high toxicity it was added to the candidate list of substances of very high concern (SVHC) in the context of EU's REACH (Europe's Registration Evaluation Authorization and Restriction of Chemicals) regulation. Due to this the use of hydrazine could be restricted or even forbidden in future.

Caused by the mentioned economic and political reasons several alternatives for hydrazine are currently under investigation. Among those "green propellants" different substances seem to fulfill the needs for a future replacement of hydrazine. The most prospective and developed candidate for low thrust systems is LMP-103S, based on ADN (ammoniumdinitramid) and developed by the Swedish company ECAPS.[2] Nevertheless other possibly prospective propellants exist. Concerning lower costs and nearly no toxicity, highly concentrated hydrogen peroxide (H_2O_2) might be a reasonable alternative.[3–5] In the USA, in China, in Russia and in Japan HAN (hydroxylammonium nitrate) based propellants are intensively studied. Those propellants offer low toxicity due to negligible vapor pressures and higher performance than conventional hydrazine.[1,6–9] The performance benefits of HAN based propellants come along with high combustion temperatures, which are challenging for catalyst material. Furthermore the so called "water propulsion" is under investigation for satellite propulsion systems.[10–12] The idea is to fuel the satellite with water and decompose it in orbit via an electrolyzer into hydrogen and oxygen. The gaseous hydrogen and oxygen are stored in separate tanks and used for thrusters at a small mixture ratio to assure low combustion temperatures. The excess oxygen is then used in cold gas thrusters. Drawbacks of water propulsion are the more complex propulsion system and the limited amount of gaseous H_2 and O_2 which have to be stored in separate tanks. Another class of prospective, low cost and high performance propellants are mixtures of nitrous oxide (N_2O) and hydrocarbons, also known as nitrous oxide fuel blends.[13,14] Here nitrous oxide and a fuel are stored monopropellant like in one tank. The mixtures offer a bipropellant like performance ($I_{sp} \geq 300$ s), while using a simplified fluid system. Additionally the components are quite cheap and non toxic. In contrast to those benefits, the main challenges are high combustion temperatures and the danger of a flashback across the injection system in the tank structure.

Several main characteristics of the named green propellants can be found in table 1. Some of the data, e.g. the TRL level and the similarity to a hydrazine propulsion system are estimations.

Currently the propellants department of DLR in Lampoldshausen is conducting research on two kinds of

Table 1. Comparison of Hydrazine to Several Green Alternatives

Propellant	$I_{sp,Vac}$ [s]	ρ [kg/m^3]	T_{cc} [K]	Similarity to HPS	TRL
Hydrazine	245[1]	1004[15]*	1227[15]	-	highest
AF-M315E	250[7]	1465-1470[7,15]	2173[15]	high	medium[7]
H_2O_2, 98 %	186**	1441*	1225**	high	high
FLP-106	255-261[16,17]	1357[17]†	1910[17]	high	low
LMP-103S	244-251[17,18]	1238[17]†	1873[17,18]	high	high[17]
Water propulsion	230[12]-350[19] ¶	997†	1000[12]	low	low[12]
NOFBX^{TM}	310[1]-345[13]	940[1]	3473[13]	low	medium[13]
N_2O&C_2H_4	303‡	879 §	3264‡	low	low

* 293.15 K and 1013 hPa

† 298.15 K and 1013 hPa

‡ Calculations by NASA CEA,[20] ϵ=40, 10 bar, ROF=6, Frozen at throat

§ ROF=6, 230 K and 25 bar[21]

¶ I_{sp} strongly depending on operation mode;[12] used ROF=0.5 and cold gas thrusters for excess oxygen

** Calculations by NASA CEA,[20] ϵ=40, 10 bar, Frozen at throat

green propellants: ADN based monopropellants[22] and mixtures of hydrocarbons with nitrous oxide (called HyNOx).[23] The following paper will show results of combustion tests with a gaseous, premixed propellant consisting of nitrous oxide (N_2O) and ethylene (C_2H_4). For conduction of the tests a modular experimental combustion chamber was used. During two test campaigns the effect of mixture ratio, chamber pressure and characteristic chamber length L^* on the characteristic exhaust velocity c^* was studied. The obtained data were compared to theoretical calculations done with NASA CEA[20] to analyze the combustion efficiency η_{c^*}.

II. Theoretical Background

A. Rocket engine performance

To evaluate the performance of a rocket propellant the characteristic velocity c^* is a commonly used parameter. By comparing the experimental c^*_{exp} to the theoretical c^*_{theo}, the c^* efficiency $\eta_{c}*$ can be derived. The c^* efficiency or combustion efficiency is used to analyze the occurring losses e.g. caused by non ideal combustion, heat fluxes, boundary layers, etc. To analyze the overall system performance and taking also nozzle effects into account, the specific impulse I_{sp} is a widely used parameter.

Compared to the specific impulse I_{sp}, the characteristic velocity c^* is mainly a function of the used propellant and the combustion chamber design and is independent on the nozzle characteristic. So by using c^* different propellant combinations and combustion chamber designs can be compared.[24] To derive the experimental c^* from test data, equation 1 is used:

$$c^* = \frac{p_{cc} \cdot A_t}{\dot{m}} \tag{1}$$

p_{cc} marks the stagnation pressure in the combustion chamber, A_t is the nozzle throat area and $\dot{m}$ is the propellant mass flow. Assuming an ideal gas, isentropic expansion and a one dimensional stationary flow field, c^* can be rewritten as:

$$c^* = \frac{\sqrt{\kappa \frac{R}{M} T_{cc}}}{\kappa \sqrt{\frac{2}{\kappa+1}^{\frac{\kappa+1}{\kappa-1}}}} = \frac{\sqrt{\frac{R}{M} T_{cc}}}{\sqrt{\kappa \left(\frac{2}{\kappa+1}\right)^{\frac{\kappa+1}{\kappa-1}}}} \tag{2}$$

T_{cc} indicates the the combustion chamber temperature, R the universal gas constant, M the molar mass of the combustion products and κ the ratio of the specific heats. For the later analysis, the experimentally obtained c^*_{exp} following equation 1 was compared to theoretical c^*_{theo} to estimate the combustion efficiency η_{c^*} of the corresponding test. The theoretical c^*_{theo} for the given mixture ratio and pressure was obtained

via NASA CEA code.[20] The c^*-efficiency was calculated via equation 3:

$$\eta_{c^*} = \frac{c^*_{exp}}{c^*_{theo}} \tag{3}$$

While the absolute c^* relates to the propellants performance, the c^* efficiency shows the losses in the combustion chamber due to heat fluxes, chemical non-equilibrium, mixture variations, losses caused by the boundary layers or non-uniformity of the flow field.

A common parameter for the general design of a combustion chamber is the characteristic combustion chamber length L^*. L^* is defined as the chamber volume divided by the nozzle throat area (equation 4). The optimum L^*_{opt} for a given chamber geometry, injection system and propellant combination is achieved, if the combustion efficiency η_{c^*} reaches a maximum.

$$L^* = \frac{V_{cc}}{A_t} \tag{4}$$

To obtain a maximum in combustion efficiency η_{c^*} two conditions must be meet:

a) The residence time of the propellant inside the combustion chamber must assure a complete or nearly complete reaction. Enough time must be available to assure proper atomization, vaporization, mixing and combustion or decomposition of the propellant.

b) The combustion gases must lose as less energy to the combustion chamber walls as possible. Heat loss, boundary layer losses and losses of the flow field should be as small as possible. A combustion chamber which allows short resident time of the combustion gases reduces these losses. E.g. a large volume to surface ratio minimizes the surface available for heat losses.

An optimum L^*_{opt} is reached if the energy losses caused by incomplete reaction and the energy losses caused by interaction with the chamber walls are at a minimum. The propellant should stays just as long in the combustion chamber to react sufficiently. Thus the optimum L^*_{opt} is connected to the time scale of the reaction and the average residence time of the propellant inside the combustion chamber.

III. Test Setup and Test Conduction

To analyze the combustion performance of the propellant, two test campaigns were conducted. The aim of the first test series was to determine which mixture ratio (ROF) delivers the highest c^* or largest combustion efficiency η_{c^*} compared to theoretical values calculated from NASA CEA.

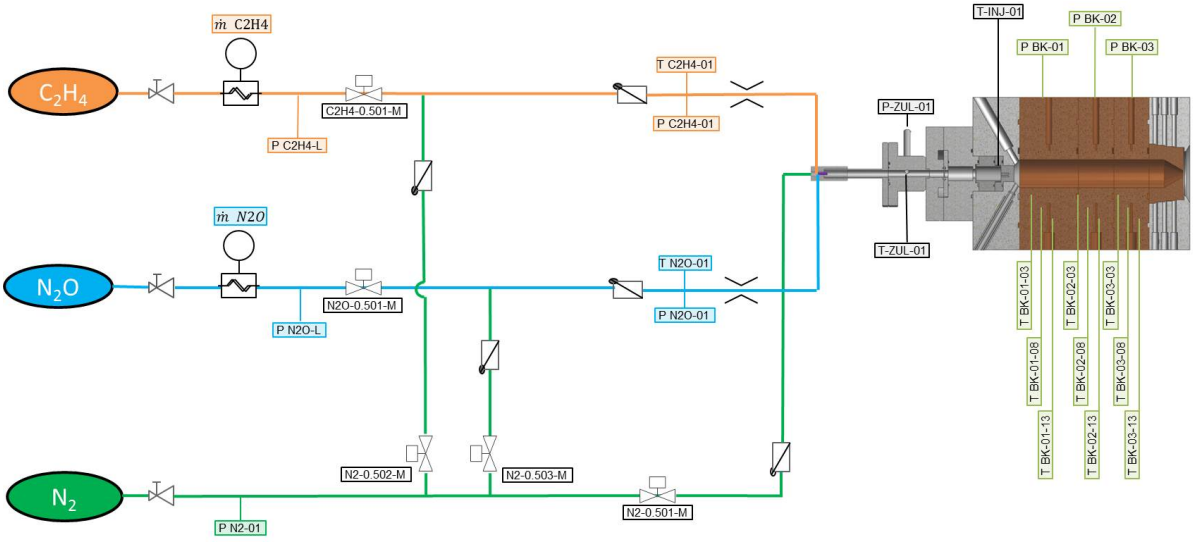

Figure 1. Simplified P&ID of the used test bench

A second campaign was performed to investigate the combustion performance depending on the characteristic combustion chamber length L^*. Additionally the effects of chamber pressure variations were analyzed. This campaign was used to investigate several assumptions made during the first test series.

To obtain more flexibility in changing the characteristic chamber length the injector faceplate was reconstructed for the second test series. A spark and glow plug used for ignition of the propellant were integrated in the faceplate. Thus the chamber length could be varied in between $L_{seg} = 0$ m and $L_{seg} = 0.110$ m. The test conduction procedure, the combustion chamber diameter, the nozzle and the injector were identically during both test campaigns.

A. Test Setup

The fluid system of the test bench is equipped with sensors for the measurement of the mass flows, the feeding pressures and the gas temperatures. During all described tests, N_2O and C_2H_4 were in gaseous state, the premixing took place upstream the injector in a tube junction. The mixture ratio and the mass flow of oxidizer and fuel were adjusted via orifices and pressure regulators downstream of the gas tanks. The mass flows in the ethylene respectively in the nitrous oxide feeding lines were measured via Coriolis mass flow meters. A simplified overview of the test bench's fluid system is shown in figure 1.

Figure 2. Test procedure

The general test procedure can be seen in figure 2. Each test was repeated twice to analyze if any anomalies occurred. During the second test campaign, the spark plug and the glow plug were used alternately to ignite the mixture.

B. First test series - Mixture ratio variation

A sectional view of the combustor used for the first test series can be seen in figure 3(a). To establish different test conditions, the chamber was designed modular: the length of the capacitive cooled chamber can easily be altered by changing or replacing the CuCrZr segments. A spark and a glow plug are available to ignite the mixture. Furthermore different injectors and flashback arresters can be tested. The nozzle segment is changeable as well, thus nozzles with different throat diameters can be tested in future.

Each combustion chamber segment is equipped with three type K thermocouples and a pressure transducer to obtain the chamber pressure and the wall temperatures during the combustion tests. The thermocouples are mounted in different radial distances to the inner combustion chamber wall and can be used to derive the heat flux during the combustion tests.

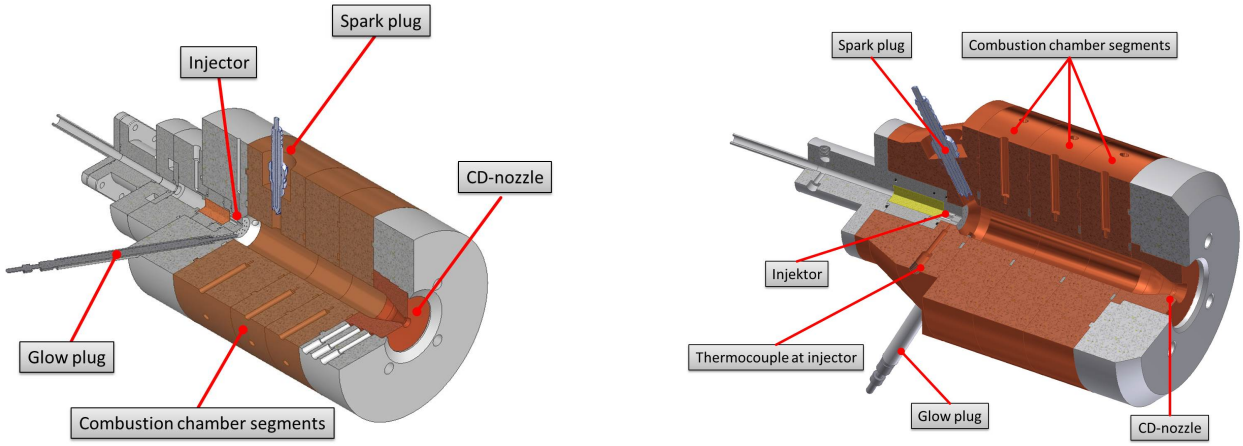

(a) Combustor design first - First test campaign

(b) Optimzed combustor design - Second test campaign

Figure 3. Combustion test of the N_2O/C_2H_4 mixture

The tests in the first series were conducted under ambient conditions with three combustion chamber segments mounted. This resulted in an overall length L_{seg} of 110 mm, the L^* for this configuration was 3.10 m. During the tests A showerhead injector was used and a conical convergent-divergent nozzle with a throat diameter of 5 mm and an expansion ratio of 1.75 was mounted. Prior to each test run, the mass flow and mixture ratio was adjusted and checked via a cold flow. The oxidizer to fuel mass ratio (ROF) was varied in between 3.8 and 12.2, while the stoichiometric mixture ratio of N_2O and C_2H_4 is 9.41. At the beginning and past each test sequence, the combustor was purged with nitrogen. Due to the capacitive cooling of the chamber the accumulated heat resulted in higher wall temperatures at the start of later test runs throughout a test series.

C. Second test campaign - Chamber length variation

Caused by the results of the first test campaign, a second test series was conducted to investigate the characteristic chamber length L^* for the used injector - chamber - propellant configuration. To be able to use all manufactured chamber segments, the injector faceplate was redesigned. The spark plug was integrated in the faceplate, so testing without any segment was possible ($L_{seg} = 0$ m). Further changes to the former design were a simplified feeding system, an optimized nozzle fitting and additional temperature measurement at the injector.

For tests without chamber segments ($L_{seg} = 0$ m), a pressure sensor was mounted at the glow plug fitting. The modified combustion chamber is shown in figure 3(b). The mixture ratio for the second test series was kept in between 5 and 7, due to the results of the primary test campaign.

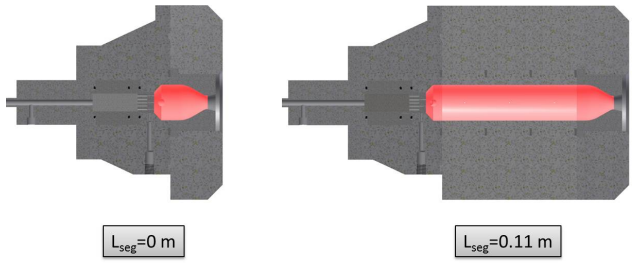

Figure 4. Two different configurations of the combustion chamber

The configuration of the combustion chamber for an L^* of 0.56 m (L_{seg}=0 m) and 3.10 m (L_{seg}=0.110 m) is shown in figure 4.

IV. Results and discussion

During the first test series the dependency of c^* and η_{c^*} on the mixture ratio (ROF) was analyzed. The mixture ratio was set prior to each test run via the mounted orifices and the adjusted pressure at the pressure regulators. Via cold flow test, the mixture ratio and the overall mass flow were checked and readjusted if required. Due to the gaseous state of the propellant and the dynamic behavior of the fluids an independent adjustment of mass flow and mixture ratio was not possible. Thus the mixture ratio was simply changed via increase or decrease of the C_2H_4 feeding pressure. This resulted in slight differences of the overall mass flow during the test runs. For the second test series, the mixture ratio (ROF) was kept in between 5 and 7 while the overall mass flow was altered during several test runs. Thus the influence of the chamber pressure on c^* was investigated.

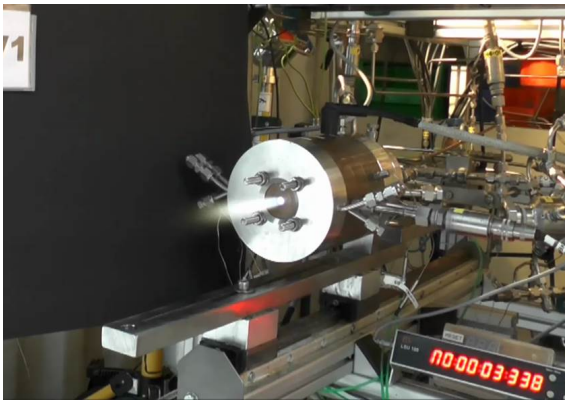

(a) Combustion test with $L* = 3.10$ m - First test campaign

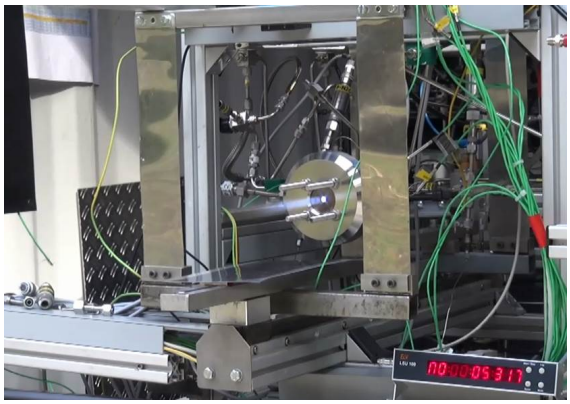

(b) Combustion test with $L* = 0.56$ m - Second test campaign

Figure 5. Combustion test of the N_2O/C_2H_4 mixture

A. First test series - Mixture ratio variation

During this test campaign, the mixture ratio and the mass flow were varied. Via pressure and mass flow data the experimental c^* values were derived. Additionally the nozzle throat diameter was measured prior and after the test runs to analyze the effect of the nozzle temperature on the throat diameter. The obtained

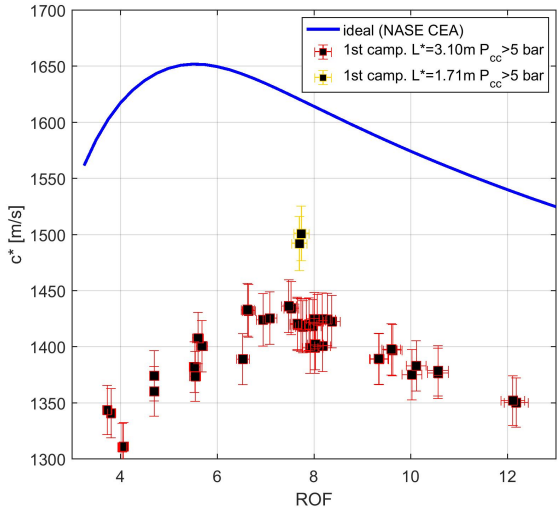

(a) c^* depending on mixture ratio

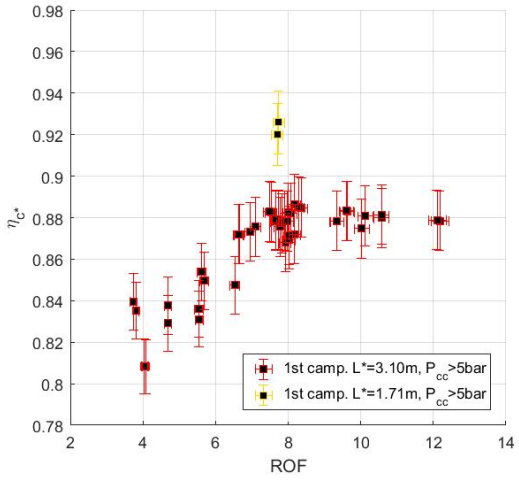

(b) η_{c^*} Efficiency depending on mixture ratio

Figure 6. c^* and η_{c^*} values for the first test campaign

c^* values for different mixture ratios (ROF) are shown in figure 6(a). The red squares mark the c^* values obtained for a characteristic chamber length L^* of 3.10 m. While the two yellow squares symbolize the corresponding c^* for an L^* of 1.71 m. The tests with a reduced chamber length were performed to investigate the influence of L^* on c^* during the last test of the first campaign. In figure 6(a) and 6(b) only tests with a chamber pressure above 5 bar are shown. For lower chamber pressures c^* dropped significantly. This was investigated more in detail during the second test campaign (see figure 8(a)).

The measured c^* for an L^* of 3.10 m is in between 1310 m/s and 1440 m/s depending on the N_2O/C_2H_4 mixture ratio. Each test run was repeated twice, due to slight deviations of the feeding pressures, the ROF and c^* are showing small differences for the two runs. Theoretical c^* values obtained by using NASA CEA[20] (reactions frozen at throat) and variation of the mixture ratio are symbolized by the blue line in the diagram 6(a).

Figure (6(b)) shows the corresponding c^* efficiency for the conducted tests. Regarding the dependency of c^* on the mixture ratio the following effects were observed:

a) The shape of the c^* curve seems to follow the development of the theoretical values in general. However, a shift of the c^* maximum to higher mixture ratios and lower absolute c^* values is clearly visible.

b) A maximum of c^* is obtained for a mixture ratio (ROF) of about 7.5. η_{c^*} shows a maximum at ROF $\approx$ 8.5. The different positions of the c^* and η_{c^*} maxima are caused by a shift in between the theoretical c^* maximum and the experimentally c^* peak value. Due to the shift, the combustion efficiency η_{c^*} for higher mixture ratios (ROF $>$ 8.5)is larger compared to the efficiency for lower mixture ratios (ROF $<$ 8.5) (see figure 6(b)).

c) The characteristic combustion chamber length L^* seems to influence the combustion performance strongly. For the test with reduced chamber length, the absolute c^* and the combustion efficiency η_{c^*} rises significantly. This is assumed to be caused by heat losses.

To analyze the heat losses to the chamber walls further calculations were performed. The heat flux density q_{loss} was obtained from former test results and calculations performed by Perakis.[25] The test conditions under which the heat flux was derived are shown in table 2. The derived heat flux density was used to reduce

Table 2. Test conditions used for heat flux calculation[25]

mass flow [g/s]	chamber pressure [bar]	mixture ratio	L^* [m]	derived heat flux [MW/m^2]
9.57	7.04	9.45	3.10	2.01

the reaction enthalpy ΔH_r^0 according to equation (5):

$$\Delta H_{r,l}^0 = \Delta H_r^0 - \Delta H_l = \sum_1^i \left[n_i \left(\Delta H_f^0 \right)_i \right]_{products} - \sum_1^i \left[n_i \left(\Delta H_f^0 \right)_i \right]_{educts} - \Delta H_l \tag{5}$$

This was achieved by reducing the standard heat of formation of nitrous oxide $\Delta H_{f,N_2O}^0$.

$$\Delta H_{l,N_2O} = \Delta H_{f,N_2O}^0 - \Delta H_l \tag{6}$$

The enthalpy loss was obtained by:

$$\Delta H_l = \frac{\dot{Q}_{loss}}{\dot{n}_{N_2O}} \tag{7}$$

While the mole flow is defined as

$$\dot{n}_{N_2O} = \frac{M_{N_2O}}{\dot{m}_{N_2O}} \tag{8}$$

The heat flux $\dot{q}_{loss}$ was multiplied by the combustion chamber surface area S_{cc} which was obtained from the CAD drawings of the chamber. So the overall heat loss $\dot{Q}_{loss}$ was calculated:

$$\dot{Q}_{loss} = \dot{q}_{loss} \cdot S_{cc} \tag{9}$$

The calculations were performed by a Matlab script, which accesses the NASA CEA program. For a variation of the mixture ratio and a for fixed heat flux the reduced c^* values were derived. Figure 7 shows the resulting c^* for different mixture ratios and different combustion chamber lengths L_{seg}.

Comparing the the heat loss calculation and the test results, the following can be observed:

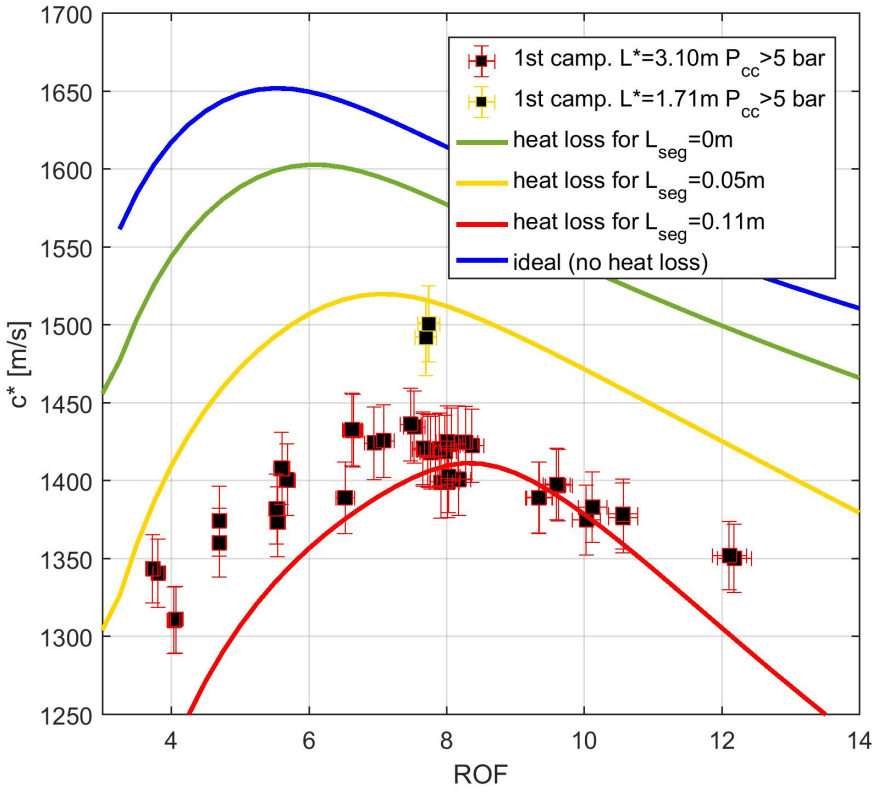

Figure 7. Calculated heat losses by using results from[25]

a) An increase in heat losses caused by a larger combustion chamber surface S_{cc} causes the c^* to drop significantly.

b) The c^* maximum shifts to regions with a higher mixture ratio when the heat losses are increases. This is caused by reduced combustion chamber temperatures T_{cc} (see 2) resulting from a reduced energy release by the combustion. Additionally the gas composition changes with combustion temperature, this alters the average molar weight of the products.

c) The heat flux used for the calculations was derived at the operation point described in table 2. For a mixture ratio of 9 to 10.5 the theoretical calculated c^* matches the experimental results in very good agreement. Even though the heat flux was derived during a different test campaign where the test conditions were slightly different (e.g. a torch igniter was used during those tests).[14] As consequence the authors assume that the reduction of c^* compared to the theoretical values is almost exclusively caused by heat losses.

d) The predicted and the measured c^* differ in the case of low and high mixture ratios. This may be caused by deviations of those test points from the test conditions where the heat flux was numerically derived (ROF=9.45). The combustion temperature is at a maximum near the stoichiometric conditions (ROF=9.41). Thus the combustion temperature and probably also the heat flux will decrease with deviations from the stoichiometric composition. Furthermore the changes in composition of the combustion gases may influence the heat flux to the chamber walls.

B. Second test campaign - Chamber length variation

Due to the results of the first test campaign, a second test series was conducted. The aim of this campaign was to analyze the influence of chamber pressure and L^* on the characteristic velocity c^*. During this tests the optimized combustion chamber was used. The length L_{seg} of the combustion chamber was reduced while the nozzle throat diameter was kept constant ($d_t = 5$mm). A reduction or exchange of combustion chamber

segments resulted in characteristic chamber lengths L^* of 3.10 m, 2.40 m, 1.71 m, 1.02 m and 0.56 m. At the beginning the chamber pressure was varied while the longest chamber configuration (L^*=3.10 m) was used. Due to these test results, the chamber pressure for the later tests was kept above 6.5 bar. The resulting c^* values for those tests are shown in figure 8(a). The mixture ratio during the second test campaign was kept in between 5 and 7.

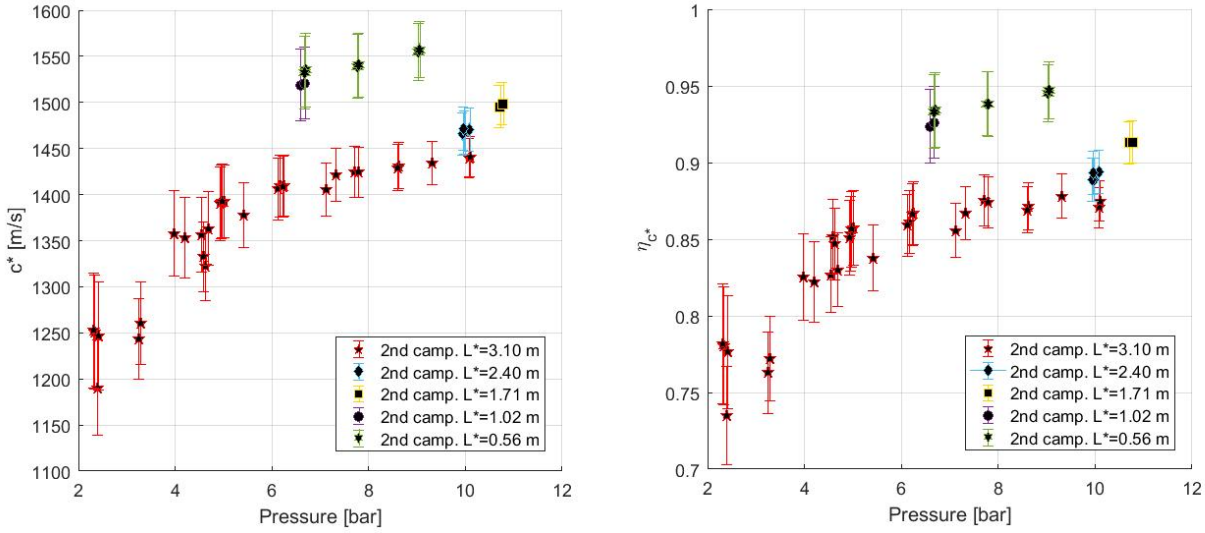

(a) Experimental c^* for variation of the pressure during the second test campaign

(b) Combustion efficiency η_{c^*} for variation of the pressure during the second test campaign

Figure 8. Experimental c^* and η_{c^*} for variation of the pressure during the second test campaign

Each color in figure 8(a) and 8(b) symbolize a used L^* configuration. The comparison of the resulting c^* values to the chamber pressure shows a strong dependency of the characteristic velocity on pressure below approximately 6 bar. For pressure levels higher than 6 bar the influence on c^* seems to decrease. The strong influence of chamber pressure on c^* for low pressure levels is assumed to be caused by the following reasons:

a) The combustion temperature is slightly reduced at low chamber pressures according to NASA CEA.[20] This results in a small reduction of c^*.

b) The amount of heat absorbed by the walls increases compared to the amount of heat produced by the combustion. For the heat flux depending on pressure the correlation:

$$\dot{q}_{loss} \propto p_{cc}^{0.68} \tag{10}$$

was derived.[25] This results in a higher heat loss to pressure ratio for low chamber pressures. E.g. the heat flux to the chamber walls decreases only by the factor of 0.62 if the chamber pressure is halved. On the other side, the heat flux increases only with a factor of 1.6 when the pressure is doubled.

c) The chemical composition of the combustion gas may change due to lower combustion temperatures and pressure levels. Possibly the molar mass of the exhaust gas increases due to lower chamber pressure.

The corresponding combustion efficiency for the second campaign can be seen in figure 8(b). The distribution of the measured c^* efficiency follows the absolute c^* curve. The combustion pressure influences the theoretical c^* only slightly so both curves show a similar behavior. A discrepancy in both figures (8(a) to 8(b)) could only be caused by different theoretical c^* values with changes in chamber pressure.

Furthermore both figures (9(a) and 9) show a significant increase in combustion efficiency η_{c^*} respectively c^* with a decrease in characteristic chamber length L^*. This supports the aforementioned assumption of heat losses mainly influencing the c^* during the test runs. The influence of chamber length on c^* and $\eta_{c^*}$is shown in figure 9 in detail.

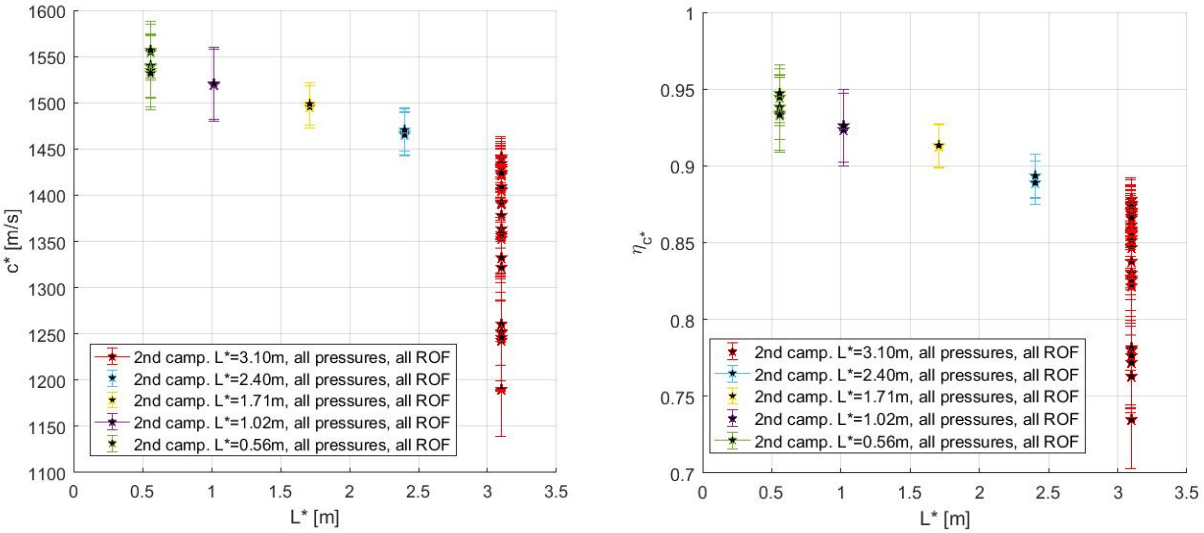

(a) c^* depending on L^*

(b) c^* Efficiency depending L^*

Figure 9. c^* and η_{c^*} depending on characteristic combustion chamber length

Both diagram show a clear influence of the chamber length on c^*. The maximum value of c^* nearly increase linear with decreasing chamber length. The broad range of c^* values for the chamber configuration with an L^* of 3.10 m results from the above mentioned variation of chamber pressures. For the test with an L^* smaller than 3.10 m the chamber pressure was kept above 6 bar, while for the test with an L^* of 3.10 the pressure was varied in between 2.3 and 10 bar (see figure 8(a)).

Due to the obtained results, the optimum chamber length L^*_{opt} is assumed to be near or below 0.56 m. For a further reduction of L^* a different set of nozzles with larger throat diameter or chamber segments with a smaller diameter have to be used. The small optimum L^*_{opt} is most likely caused by the premixed, gaseous state of the propellant. Due to this state the propellant does no require any time for atomization, vaporization and mixing before the combustion can start.

C. Error analysis

The error bars in the shown diagrams were derived by an deviation analysis according to JANNAF.[26] The procedure to derive the deviations is described below. The obtained static pressure data from the sensors was corrected by the average Mach number in the combustion chamber according to.[27] The isentropic coefficient for calculation the Mach number in the combustion chamber was taken from NASA CEA. Due to the large contraction ratio $\epsilon_c = 23.08$ the stagnation pressure differed only by 0.04 % from the measured static pressure. The data obtained from the pressure sensors were compared to a reference device, equipped with a calibrated Beamex pressure module (Beamex MC5 EXT 250). The maximum deviation of the sensors to the pressure module was 0.79 %. The coriolis mass flow sensors (Rehonik RHM015 and Emerson CFM025) were calibrated by the manufacturer. Due to the calibration certificate their nominal deviation was 0.5 %. To counter check the Coriolis sensors, both were mounted in a row and a gaseous nitrogen mass flow was applied. The deviation in between both sensors exceeded the maximum deviation given by the manufacturer (deviation $\leq$ 1.44 %). Because all installation requirements were met the difference in the measurements of the two mass flow meters is assumed to be caused by the reference calibration with water. Possibly the calibration with an incompressible fluid leads to bigger deviations in the sensors' data when run with compressible gases. The nozzle throat diameter was measured during the test runs with a calibrated micrometer. The change in diameter depending on temperature of the nozzle was investigated, no noticeable change of the throat size was observed. This might be caused by the relatively inelastic stainless steel fitting of the nozzle and the low combustion chamber wall temperatures during the test runs (up to 250C) Table 3 shows the maximum measurement deviations of the sensors and the average diameter of the nozzle.

Table 3. Maximum observed deviations and average nozzle throat diameter

Measured value	max. deviation/average diameter
pressure	0.79 %
mass flow	1.44 %
nozzle throat diameter	4.995 [mm]

The deviations in mass flow, chamber pressure and nozzle throat diameter were used to calculate the uncertainty of c^* and η_{c^*} according to:

$$u_y = \sqrt{\left(\frac{\partial y}{\partial x_1} \cdot u_1\right)^2 + \left(\frac{\partial y}{\partial x_2} \cdot u_2\right)^2 + ...} \tag{11}$$

For example u_y symbolizes the deviation of c^* while u_1 and u_2 are the absolute deviations for pressure and mass flow. Those absolute deviations were calculated by multiplying the deviation in percent (table 3) with the average value of the measured pressure or mass flow during a test run.

V. Summary and Outlook

Combustion tests with a premixed green propellant consisting of nitrous oxide (N_2O) and ethylene (C_2H_4) were conducted. Both gases were premixed upstream the injector of an experimental combustion chamber. The scope of a first test series was to derive the c^* values and the c^* efficiency depending on the oxidizer to fuel ratio (ROF). During this first test series c* efficiencies up to 88 % were obtained. The low combustion efficiency led to a second test campaign, where the characteristic chamber length L^* and the according heat losses to the chamber walls were investigated. Additionally the influence of combustion chamber pressure on c^* was investigated. Furthermore the theoretical c^* values calculated via NASA CEA were reduced by the heat flux to the chamber walls. The heat flux density was obtained from previous tests and corresponding heat flux calculations.[25] During the tests the following results and correlations were found:

a) A maximum c^* of 1430 m/s at ROF=7.5 for $L* = 3.10$m could be reached. Reducing the L^* to 0.56 m resulted in a maximum L^* of 1550 m/s for a mixture ratio of 6.7. With a c^* of 1550 m/s a combustion efficiency of $\approx$ 95 % was achieved.

b) With an increase in heat loss, the maximum value for c^* is lowered and shifted to zones with higher mixture ratios. This can be simulated by reducing the reaction enthalpy, respectively the heat of formation of the educts in NASA CEA. The heat loss to the chamber walls effect the average chamber temperature and thus leads to a reduction of c^*. Additionally the composition of the burned gas changes with combustion temperature.

c) Reducing the theoretical c^* by the derived heat flux for a specific test point leads to a very good prediction of the experimental c^*. Due to this it is assumed that heat losses are the most influencing factor on combustion efficiency for the described tests.

d) A chamber pressure below 6 bar reduces c^* significantly. Above 6 bar an increase in pressure effects the c^* only slightly. The low efficiency at reduced pressure levels might be caused by an increase in the heat flux to pressure ratio. During prior tests the correlation:[14,25]

$$\dot{q} \propto p^{0.68} \tag{12}$$

was derived. Thus for low pressure levels the heat flux increases disproportionately.

e) A reduction of the chamber length down to L^*=0.56 m showed significant increase in c^* and ${\eta_c}^*$. This rise in c^* is most likely caused by a reduction of the chamber surface and an corresponding reduction of the total heat flux. The combustion process seems to be completed close to the injector due to the premixed, gaseous state of the propellant.

In future tests the effects of a further reduced characteristic chamber length L^* will be studied. To achieve a smaller L^* additional nozzles will be used. Further on, test with liquefied gases are planned. The influence of the evaporation on the combustion efficiency will then be studied in detail.

VI. Acknowledgment

The authors would like to thank the M11 test bench team for the support in preparing and conducting the tests. The work described in this paper was conducted in the framwork of DLR's Future Fuels project.

References

[1]Sackheim, R. L. and Masse, R. K., "Green Propulsion Advancement: Challenging the Maturity of Monopropellant Hydrazine," *Journal of Propulsion and Power*, Vol. 30, No. 2, 2014, pp. 265–276.

[2]Gohardani, A. S., Stanojev, J., Demairé, A., Anflo, K., Persson, M., Wingborg, N., and Nilsson, C., "Green space propulsion: Opportunities and prospects," *Progress in Aerospace Sciences*, Vol. 71, 2014, pp. 128–149.

[3]Kajon, D., Masson, F., Wagner, T., Welberg, D., Büchner da Costa, T., and Mansouri, J., "Development of an Attitude Control and Propellant Settling System for the aA5ME Upper Stage: Space Propulsion Conference," 19 - 22 May 2014.

[4]Gotzig, U., Kraus, S., Welberg, D., Fiot, D., Michaud, P., Desaguier, C., Casu, S., Geiger, B., and Kiemel, R., "Development and Test of a 3D printed Hydrogen Peroxide Flight Control Thruster," *51st AIAA/SAE/ASEE Joint Propulsion Conference, 27.-29. July 2015, Orlando, Florida, USA*.

[5]Božić, O., Porrmann, D., Lancelle, D., and May, S., "Enhanced development of a catalyst chamber for the decomposition of up to 1.0 kg/s hydrogen peroxide," *CEAS Space Journal*, Vol. 8, No. 2, 2016, pp. 77–88.

[6]Fukuchi, A. B., Nagase, S., Maruizumi, H., and Ayabe, M., "HAN/HN-Based Monopropellant Thrusters," *IHI Engineering Review*, Vol. 43, 2010, pp. 22–28.

[7]Spores, R. A., "GPIM AF-M315E Propulsion System," *51st AIAA/SAE/ASEE Joint Propulsion Conference, 27.-29. July 2015, Orlando, Florida, USA*.

[8]Katsumi, T., Inoue, T., Nakatsuka, J., Hasegawa, K., Kobayashi, K., Sawai, S., and Hori, K., "HAN-based green propellant, application, and its combustion mechanism," *Combustion, Explosion, and Shock Waves*, Vol. 48, No. 5, 2012, pp. 536–543.

[9]Robert S. Jankovsky, "HAN-Based Monopropellants Assessment for Spacecraft: NASA Technical Memorandum 107287: AIAA-96-2863," .

[10]Konstantin Manassis, *Development of a GOX/GH2 propulsion thruster*, Bachelorthesis, University of Stuttgart, Stuttgart, 2015.

[11]Nicolas Harmansa, *Design of a Low-Cost Propulsion System based on Water Electrolysis*, Masterthesis, University of Stuttgart, Stuttgart, 2015.

[12]S. Pérez Roca, *Water-electrolysis Propulsion for Spacecraft Applications: Breadboard Development, Simulation and Demonstration*, Master thesis, ISAE Supaero, Sept. 2016.

[13]Mungas, G., Vozoff, M., and Rishikof, B., "NOFBX: A new non-toxic, Green propulsion technology with high performance and low cost: 63rd International Astronautical Congress," *63rd International Astronautical Congress, 1-5 October 2012, Naples, Italy*.

[14]Werling, L., Perakis, N., Müller, S., Hauck, A., and Ciezki, Helmut and Schlechtriem, Stefan, "Hot firing of a N2O/C2H4 premixed green propellant: first combustion tests and results," *Space Propulsion Conference, 1.-5. May 2016, Rome, Italy*.

[15]Ferran, V.-B. and Smith, M., "Replacement of Conventional Spacecraft Propellants with Green Propellants," *Space Propulsion Conference 7.-10 May 2012, Bordeaux, France*.

[16]Wingborg, N., Johansson, M., and Bodin, L., "Initial development of a laboratory rocket thruster for ADN-based liquid monopropellants," .

[17]Gohardani, A. S., Stanojev, J., Demairé, A., Anflo, K., Persson, M., Wingborg, N., and Nilsson, C., "Green space propulsion: Opportunities and prospects," *Progress in Aerospace Sciences*, Vol. 71, 2014, pp. 128–149.

[18]Neff, K., King, P., Anflo, K., and Möllerberg, R., "High performance green propellant for satellite applications: 45th AIAA/ASME/SAE/ASEE Joint Propulsion Conference & Exhibit," 2-5 August 2009.

[19]Wim A. de Groot, Lynn A. Arrington, James F. McElroy, Fred Mitlitsky, Andrew H. Weisberg, Preston H. Carter I, and Blake Myers and Brian D. Reed, "Electrolysis Propulsion for Spacecraft Applications," .

[20]Gordon, S. and McBride, B., *Computer Program for Calculation of Complex Chemical Equilibrium Compositions and Applications: NASA Reference Publication 1311: I. Analysis*, 1996.

[21]E. W. Lemmon and M. L. Huber and M. O. McLinden, "NIST Standard Reference Database 23: Reference Fluid Thermodynamic and Transport Properties-REFPROP," 2013.

[22]Negri, M., "Replacement of Hydrazine: Overview and First Results of the H2020 Project Rheform," *6th European Conference for Aeronautics and Space Sciences (EUCASS), 29.06-03.7.2015, Krakow, Poland*.

[23]Werling, L., Perakis, N., Müller, S., Hauk, A., Ciezki, H., and Schlechtriem, S., "Hot firing of a N2O/C2H4 premixed green propellant: First combustion tests and results," *Space Propulsion Conference, 1.-5. May 2016, Rome, Italy*.

[24]Sutton, G. P. and Biblarz, O., *Rocket propulsion elements*, John Wiley & Sons, 2010.

[25]Nikolaos Perakis, Lukas Werling, Helmut Ciezki, and Stefan Schlechtriem, "Numerical Calculation of Heat Flux Profiles in a N2O/C2H4 Premixed Green Propellant Combustor using an Inverse Heat Conduction Method," *Space Propulsion Conference, 1.-5. May 2016, Rome, Italy*.

[26]DIN 1319-4, "Grundbegriffe der Meßtechnik; Behandlung von Unsicherheiten bei der Auswertung von Messungen," 1996-02-01.

[27]Johns Hopkins University, *Jannaf Rocket Engine Performance Prediction and Evaluation Manual*, CPIA publication, Chemical Propulsion Information Agency, 1975.